Thiolato-Bridged Dinuclear d^8 Iridium(I) Complexes and Their Hydrogenation to Form Dihydridodiiridium(II)(*Ir–Ir*) Complexes.[1] Crystal and Molecular Structures of $[Ir(\mu\text{-St-Bu})(CO)(P(OMe)_3)]_2$ and of $[Ir(H)(\mu\text{-St-Bu})(CO)(P(OMe)_3)]_2$

J. J. Bonnet, A. Thorez, A. Maisonnat, J. Galy, and R. Poilblanc*

Contribution from the Laboratoire de Chimie de Coordination du CNRS, associé à l'Université Paul Sabatier, 31030 Toulouse-Cedex, France.
Received March 19, 1979

Abstract: A series of thiolato-bridged dinuclear d^8 iridium(I) complexes $[Ir(\mu\text{-St-Bu})(CO)(PR_3)]_2$ with R = Me, Ph, NMe_2, or OMe reacts irreversibly with molecular hydrogen to yield quantitatively thiolato-bridged dihydridodiiridium complexes $[Ir(H)(\mu\text{-St-Bu})(CO)(PR_3)]_2$ in which, as shown by spectroscopic evidence, one hydrogen atom is bound to each iridium atom. The hydrido species can be protonated giving $\{[Ir(H)(\mu\text{-St-Bu})(CO)(PR_3)]_2H\}^+$ complexes in which the added proton occupies a bridging position between the two iridium atoms, suggesting the existence of a two-electron Ir–Ir bond in the starting compounds. Crystal structure determinations of $[Ir(\mu\text{-St-Bu})(CO)(P(OMe)_3)]_2$ and $[Ir(H)(\mu\text{-St-Bu})(CO)(P(OMe)_3)]_2$ have been performed. In the former compound, each iridium atom has a square-planar coordination. The dihedral angle between the two planes is 123.2°, and the Ir–Ir separation is 3.216 (2) Å. The *t*-Bu groups are in an anti configuration with respect to the Ir_2S_2 dihedral angle of the Ir–Ir axis. The phosphite and carbonyl ligands are in a cis arrangement. The compound crystallizes in the orthorhombic space group D_2^4-$P2_12_12_1$ in a cell of dimensions a = 13.017 (1), b = 21.300 (1), and c = 10.203 (1) Å with Z = 4. Based on 1339 unique reflections having $F_o^2 \geq 3\sigma(F_o^2)$, the structure was refined (on F) by full-matrix least-squares techniques to conventional agreement indices of R = 0.044 and R_w = 0.041. In the dihydrido compound, each iridium atom has a rectangular pyramidal environment. The phosphite ligand occupies the axial position. The molecule has a crystallographically imposed mirror plane. The *t*-Bu groups are in a syn-endo configuration with respect to the Ir_2S_2 core. A distance of 2.673 (1) Å between the two iridium atoms, together with other structural features, indicates the presence of an Ir–Ir single bond. The compound crystallizes in the monoclinic C_{2h}^2-$P2_1/m$ space group in a cell of dimensions a = 9.675 (2) Å, b = 19.060 (6) Å, c = 7.778 (2) Å, and β = 94.30 (2)°. Based on 2618 unique reflections having $F_o^2 \geq 3\sigma(F_o^2)$, the structure was refined by full-matrix least-squares techniques to conventional agreement indices of R = 0.056 and R_w = 0.065. Pathways for the formation and isomerization of the dihydride complexes are proposed.

Introduction

Considerable interest has arisen in the design, the synthesis, and the reactivity of novel polynuclear metal complexes particularly in view of their potential roles in homogeneous catalysis.[2] In this context, the search for cooperative interaction can be considered as a possible inductive approach.[3]

Following our studies on the reactivity of dinuclear bridged d^8 metal complexes, we describe in this paper the addition of molecular hydrogen to $[Ir(\mu\text{-St-Bu})(CO)(PR_3)]_2$, **1** (R = Me, Ph, NMe_2, or OMe), which leads to dihydrido species $[Ir(H)(\mu\text{-St-Bu})(CO)(PR_3)]_2$, **2**, with a Ir–Ir single bond. The protonation of the dihydrido complexes was followed by IR and NMR spectroscopies. In order to clarify the structural implications of the addition of molecular hydrogen to **1**, we determined X-ray crystallographic characterizations of **1** (R = OMe) and **2** (R = OMe).

Experimental Section

All reactions were carried out under a dry and oxygen-free dinitrogen atmosphere using Schlenk tubes and vacuum-line procedures. Solvents (hexane, toluene, dichloromethane, and chloroform) were dried and freed of molecular oxygen. Microanalyses were performed by the Service Central de Microanalyses du CNRS. Molecular weights were measured in benzene using a Mechrolab osmometer. Conductivities were determined for 10^{-3} equiv L^{-1} solutions in methanol with an Industrial conductivity bridge instrument. Infrared spectra were recorded in hexadecane or dichloromethane solutions or cesium bromide pellets, using a Perkin-Elmer 225 spectrometer; in the carbonyl stretching region, the spectra were calibrated with water vapor lines. ^{1}H NMR spectra were obtained at 90 MHz on a Bruker WH90 spectrometer, in the FT mode, and at 250 MHz on a Cameca equipped with variable-temperature probes. Chemical shifts were measured with respect to internal Me_4Si and are reported on the τ scale. Proton noise decoupled ^{31}P NMR spectra were performed at 36.4 MHz on a Bruker WH90 spectrometer. Chemical shifts were measured with respect to external H_3PO_4 and are given in parts per million, downfield positive. Optical spectra were recorded from 600 to 300 nm with a Cary 14 spectrophotometer from dichloromethane solutions. The starting materials **1** were prepared as previously reported[4] and recrystallized from hexane solution with a yield of 80%.

Absorption of Hydrogen or Deuterium by $[Ir(\mu\text{-St-Bu})(CO)(PR_3)]_2$, 1 (R = Me, Ph, NMe_2 or OMe), Complexes. In a hydrogenation apparatus, 5 mL of toluene was saturated with hydrogen at 1 atm pressure. Then a toluene solution of $[Ir(\mu\text{-St-Bu})(CO)(PR_3)]_2$ was introduced and the additional hydrogen uptake measured. For a complex concentration of 0.011 mol L^{-1}, the rate of uptake varied with R. The reaction time varied from 30 min (R = Me) to 3 h (R = OMe). In all cases, the absorption was found to correspond to 1 mol of hydrogen per mol of the starting dinuclear material.

Preparation of $[Ir(H)(\mu\text{-St-Bu})(CO)(P(OMe)_3)]_2$. A solution of $[Ir(\mu\text{-St-Bu})(CO)(P(OMe)_3)]_2$ (0.623 g) in degassed hexane (15 mL) was allowed to absorb hydrogen for 3 h at room temperature. The solution changed from orange to pale yellow. Yellow plates (0.468 g, 75%) were obtained on concentrating the hexane solution.

Anal. Calcd for $C_{16}H_{38}Ir_2O_8P_2S_2$: C, 22.1; H, 4.42; S, 7.38. Found: C, 22.4; H, 4.39; S, 7.09.

Preparation of $[Ir(H)(\mu\text{-St-Bu})(CO)(PPh_3)]_2$. A solution of $[Ir(\mu\text{-St-Bu})(CO)(PPh_3)]_2$ (0.328 g) in degassed toluene (20 mL) was allowed to absorb hydrogen at room temperature for 2 h. On concentrating the toluene solution, the title complex was obtained as yellow plates (0.272 g, 77%) with one toluene solvate molecule per molecule of complex. The 1:1 ratio was deduced by ^{1}H NMR spectroscopy by integrating the methyl against the *tert*-butyl resonances.

Anal. Calcd for $C_{53}H_{58}Ir_2O_2P_2S_2$: C, 51.4; H, 4.73; S, 5.18. Found: C, 52.2; H, 4.94; S, 5.23.

Recrystallization of the above product in hexane gave the dihydrido complex solvent-free.

0002-7863/79/1501-5940$01.00/0

Anal. Calcd for $C_{46}H_{50}Ir_2O_2P_2S_2$: C, 48.2; H, 4.41; S, 5.60; mol wt, 1145. Found: C, 48.0; H, 4.28; S, 4.96; mol wt. 1185.

Preparation of [Ir(D)(μ-St-Bu)(CO)(PPh₃)]₂. This deuterated compound was prepared similarly using D_2.

Anal. Calcd for $C_{53}H_{56}D_2Ir_2O_2P_2S_2$: C, 51.4; H, 4.56; D, 0.32; S, 5.17. Found: C, 51.4; H, 4.78; D, 0.43; S, 5.19.

Preparation of $[Ir(H)(\mu\text{-St-Bu})(CO)(P(NMe_2)_3)]_2$ and $[Ir(H)(\mu\text{-St-Bu})(CO)(PMe_3)]_2$. These two compounds were prepared in a similar way in hexane solution. Yellow crystals were obtained in both cases from hexane solutions with yields ranging from 75 to 80%.

2 (R = NMe_2). Anal. Calcd for $C_{22}H_{56}N_6Ir_2O_2P_2S_2$: C, 27.9; H, 5.97; N, 8.87; S, 6.77. Found: C, 28.3; H, 5.90; N, 8.74; S, 6.62. **2** (R = Me). Anal. Calcd for $C_{16}H_{38}Ir_2O_2P_2S_2$: C, 24.9; H, 4.97; S, 8.29. Found: C, 25.0; H, 4.98; S, 8.19.

Preparation of $\{[Ir(H)(\mu\text{-St-Bu})(CO)(P(OMe)_3)]_2(H)\}^+ ClO_4^-$. To a solution of $[Ir(H)(\mu\text{-St-Bu})(CO)(P(OMe)_3)]_2$ (0.330 g) in ethanol (10 mL), a large excess of perchloric acid (ca. 500 μL of 60% perchloric acid solution) was added. The initially yellow solution quickly turned colorless. Concentration of the solution in vacuo gave fine, white crystals of the required compound. The product was filtered off, washed with water, and dried in vacuo (0.293 g, 80%). It may be recrystallized from methanol or ethanol solution to give thin, white needles.

Anal. Calcd for $C_{16}H_{39}ClIr_2O_{12}P_2S_2$: C, 19.82; H, 4.06; S, 6.61. Found: C, 19.85; H, 4.06; S, 5.81. Conductivity $\Lambda = 92.2\ \Omega^{-1}\ cm^2\ mol^{-1}$.

Preparation of $\{[Ir(D)(\mu\text{-St-Bu})(P(OMe)_3)]_2(H)\}^+ClO_4^-$, $\{[Ir(H)(\mu\text{-St-Bu})(CO)(PPh_3)]_2(H)\}^+ClO_4^-$, and $\{[Ir(H)(\mu\text{-St-Bu})(CO)(PMe_3)]_2(H)\}^+ClO_4^-$. All these compounds were prepared similarly with comparable yields.

$\{[Ir(D)(\mu\text{-St-Bu})(CO)(P(OMe)_3)]_2(H)\}^+ClO_4^-$. Anal. Calcd for $C_{16}H_{37}ClD_2Ir_2O_{12}P_2S_2$: C, 19.78; H, 3.85; D, 0.41; S, 6.60. Found: C, 19.84; H, 3.94; D, 0.40; S, 5.97. Conductivity $\Lambda = 85.1\ \Omega^{-1}\ cm^2\ mol^{-1}$.

$\{[Ir(H)(\mu\text{-St-Bu})(CO)(PPh_3)]_2(H)\}^+ClO_4^-$. Anal. Calcd for $C_{46}H_{51}ClIr_2O_6P_2S_2$: C, 44.3; H, 4.13; S, 5.15. Found: C, 44.5; H, 4.38; S, 5.34. Conductivity $\Lambda = 104\ \Omega^{-1}\ cm^2\ mol^{-1}$.

Collection and Reduction of the X-ray Data. Preliminary film data on Weissenberg and precession cameras showed the crystals of $[Ir(\mu\text{-St-Bu})(CO)(P(OMe)_3)]_2$, **1** (R = OMe), to belong to the orthorhombic system and those of $[Ir(H)(\mu\text{-St-Bu})(CO)(P(OMe)_3)]_2$, **2** (R = OMe), to the monoclinic system. Systematic absences ($h00$, $h = 2n + 1$; $0k0$, $k = 2n + 1$; $00l$, $l = 2n + 1$) lead to the $P2_12_12_1$ (D_2^4) space group for **1** (R = OMe); for **2** (R = OMe), the absences ($0k0$, $k = 2n + 1$) lead to the $P2_1(C_2^2)$ noncentrosymmetric or $P2_1/m(C_{2h}^2)$ centrosymmetric space group. The centrosymmetric C_{2h}^2-$P2_1/m$ for **2** (R = OMe) was shown to be the correct choice on the basis of refinement of the structure with acceptable positional parameters, thermal parameters, and agreement indices. Table I gives pertinent details of the crystals and data collections. Data collections were carried out on a CAD4 Nonius diffractometer. Background counts were measured at both ends of the scan range using a ω–2θ scan equal, at each side, to one-fourth of the scan range of the peak. In this manner, the total duration of measuring backgrounds is equal to half of the time required for the peak scan. The intensities of four standard reflections were measured every 2 h of X-ray exposure for both compounds **1** and **2** (R = OMe). The intensities of 4600 ($h, k, l \geq 0$) reflections were measured at 22 °C out to $2\theta = 60°$ using Mo Kα radiation for **1** (R = OMe). The intensities of 4497 ($+h, +k, \mp l$) reflections were measured at 22 °C out to $2\theta = 60°$ using Mo Kα radiation for **2** (R = OMe). A value of $p = 0.03$ was used in both cases in the calculation of $\alpha(F_o^2)$.[5] Of the 4600 unique reflections for **1** (R = OMe), 1339 have $F_o^2 > 3\sigma(F_o^2)$ and were used for subsequent calculations. Of the 4497 reflections measured for **2** (R = OMe), 4123 are unique and 2618 have $F_o^2 > 3\sigma(F_o^2)$ and were used for subsequent calculations.

Solution and Refinement of the Structures. For both complexes **1** and **2** (R = OMe), the Ir, P, and S atoms were readily located from a Patterson synthesis. Full-matrix least-squares refinement and difference Fourier maps were used to locate all remaining nonhydrogen atoms. The quantity minimized was $\Sigma w(|F_o| - |F_c|)^2$ where $|F_o|$ and $|F_c|$ are the observed and calculated structure amplitudes and where the weights, w, are taken as $4F_o^2/\sigma^2(F_o^2)$. The agreement indices are defined as $R = \Sigma(||F_o| - |F_c||)/|F_o|$ and $R_w = (\Sigma w(|F_o| - |F_c|)^2/\Sigma w|F_o|^2)^{1/2}$. The atomic scattering factors were taken from the usual tabulation.[6] The effects of anomalous dispersion were included in F_c for Ir, P, and S using Cromer and Ibers'[7] values of $\Delta f'$ and $\Delta f''$. Two tables of observed and calculated structure factors for **1** and **2** (R = OMe) are available.[8] All nonhydrogen atoms were refined anisotropically. The hydride ligand of **2** (R = OMe) has not been located in a difference Fourier map but has been included as a fixed contribution in the final cycle of refinement. Its position has been assumed to be in the vacant site of coordination around Ir (i.e., in the equatorial plane containing the two bridging sulfur atoms and the C(1) carbon atom of the carbonyl group). The Ir–H distance has been assumed to be 1.70 Å, which seems realistic.[19] The final positional and thermal parameters of the atoms appear in Tables II and III. Tables IV and V contain the root mean square amplitudes of vibration.[8]

Table I. Summary of Crystal Data and Intensity Collection

compd	**1**, R = OMe	**2**, R = OMe
formula	$C_{16}H_{36}S_2P_2Ir_2O_8$	$C_{16}H_{38}S_2P_2Ir_2O_8$
formula weight	866.93 amu	868.95 amu
a	13.017 (1) Å	9.675 (2) Å
b	21.300 (1) Å	19.060 (6) Å
c	10.203 (1) Å	7.778 (2) Å
β		94.30 (2)°
V	2828.9 Å³	1430.3 Å³
Z	4	4 (half molecule)
density (calcd)	2.03 g cm⁻³	1.98 g cm⁻³
density (measured in aqueous ZnI_2)	2.01 g cm⁻³	1.96 g cm⁻³
space group	D_2^4-$P2_12_12_1$	C_{2h}^2-$P2_1/m$
crystal dimension	0.260 × 0.214 × 0.060 mm	0.312 × 0.270 × 0.245 mm
boundary faces of the prism	{001, 100, 001}	{100, 0$\bar{1}$1, 01$\bar{1}$}
crystal volume	3.34×10^{-3} mm³	2.06×10^{-2} mm³
temp	22 °C	22 °C
radiation	Mo Kα (0.7093 Å) from monochromator	Mo Kα (0.7093 Å) from monochromator
linear absorption factor	102.8 cm⁻¹	98.5 cm⁻¹
transmission factors	0.169–0.544	0.212–0.375
take-off angle	3.5°	3.8°
2θ limits	3–60°	4–60°
final no. of variables	152	146
unique data used	1339$F_o^2 \geq 3\sigma(F_o^2)$	2618$F_o^2 \geq 3\sigma(F_o^2)$
quantity minimized	$\Sigma w(\|F_o\| - \|F_c\|)^2$	$\Sigma w(\|F_o\| - \|F_c\|)^2$
weight	$w = 4F_o^2/\sigma^2(F_o^2)$	$w = 4F_o^2/\sigma^2(F_o^2)$
$R = \Sigma\|\|F_o\| - \|F_c\|/\Sigma\|F_o\|$	0.044	0.056
$R_w = (\Sigma w(\|F_o\| - \|F_c\|)^2/\Sigma wF_o^2)^{1/2}$	0.041	0.065
standard error in an observation of unit weight	1.25 e	1.79 e

Results

The addition of molecular hydrogen to the complexes $[Ir(\mu\text{-St-Bu})(CO)(PR_3)]_2$, **1** (R = Me, Ph, NMe_2, or OMe), in toluene, hexane, or methanol solutions irreversibly yields diamagnetic[10] dihydrido dinuclear species $[Ir(H)(\mu\text{-St-Bu})(CO)(PR_3)]_2$, **2.**

Assignment of the Configurations of Complexes 2 in Solution. Infrared and NMR Studies: The hydrogenation of complexes **1** is accompanied by a shift of ca. 20–30 cm⁻¹ of the ν(CO) bands toward higher frequencies in the IR spectra. The occurrence of three ν(CO) bands (Table VI) is consistent with the presence of more than one isomeric form of the dihydride species. The ν(IrH) vibrations appear in the terminal Ir–H region, i.e., 2100–2200 cm⁻¹. Treatment of **1** with deuterium

Table II. Positional and Thermal Parameters for the Atoms of $(Ir^{I}(\mu\text{-Sr-Bu})(CO)(P(OCH_3)_3))_2$[a]

ATOM	X	Y	Z	B11 OR B(A²)	B22	B33	B12	B13	B23
IR(1)	0.15344(10)	0.27171(8)	0.57535(12)	58.3(10)	21.2(5)	59.9(13)	0.8(6)	2.6(13)	3.6(8)
IR(2)	0.05627(11)	0.40546(8)	0.65287(14)	52.9(9)	23.6(5)	100.9(18)	1.0(6)	3.0(13)	-2.9(9)
S(1)	0.1810(6)	0.3409(5)	0.7568(8)	54.(6)	27.(3)	55.(9)	-6.(4)	6.(6)	4.(5)
S(2)	0.1502(7)	0.3699(4)	0.4629(8)	67.(6)	22.(3)	98.(11)	-6.(4)	-6.(9)	-2.(5)
P(1)	0.1320(7)	0.2238(5)	0.3852(8)	82.(8)	19.(3)	98.(12)	9.(4)	7.(8)	-5.(5)
P(2)	-0.0481(8)	0.4600(6)	0.5262(12)	64.(8)	35.(4)	203.(19)	-6.(5)	28.(11)	-11.(8)
O(1)	0.1415(20)	0.1497(13)	0.7014(22)	7.2(7)					
O(2)	-0.0603(24)	0.4458(14)	0.8864(27)	9.2(9)					
O(3)	0.2246(15)	0.2263(11)	0.2881(18)	4.3(5)					
O(4)	0.1032(17)	0.1516(12)	0.3990(23)	6.0(6)					
O(5)	0.0480(15)	0.2522(10)	0.2850(18)	3.7(5)					
O(6)	-0.0165(18)	0.5245(14)	0.4694(23)	6.9(7)					
O(7)	-0.1571(21)	0.4722(13)	0.5912(26)	8.7(7)					
O(8)	-0.0910(24)	0.4259(17)	0.395(4)	12.0(11)					
C(1)	0.1465(27)	0.2032(18)	0.646(3)	5.5(9)					
C(2)	-0.016(4)	0.4276(25)	0.781(5)	11.3(17)					
C(3)	0.1500(26)	0.3055(15)	0.922(3)	4.7(7)					
C(4)	0.0447(24)	0.2756(17)	0.928(3)	5.1(8)					
C(5)	0.2362(24)	0.2557(17)	0.957(3)	5.4(9)					
C(6)	0.1581(27)	0.3643(17)	1.0156(29)	4.9(8)					
C(7)	0.2752(27)	0.4132(20)	0.444(4)	6.0(10)					
C(8)	0.3474(28)	0.3667(18)	0.374(3)	6.3(10)					
C(9)	0.320(3)	0.4355(21)	0.567(4)	9.2(13)					
C(10)	0.2510(29)	0.4664(19)	0.345(4)	7.7(11)					
C(11)	0.3231(27)	0.1946(18)	0.328(4)	6.9(10)					
C(12)	0.085(3)	0.1104(22)	0.281(4)	8.6(13)					
C(13)	-0.0530(26)	0.2651(18)	0.327(3)	6.2(9)					
C(14)	-0.050(5)	0.4274(28)	0.275(5)	13.5(20)					
C(15)	-0.241(3)	0.5075(24)	0.521(4)	8.5(12)					
C(16)	0.0332(29)	0.5738(20)	0.558(4)	8.0(12)					

[a] Estimated standard deviations in the least significant figure(s) are given in parentheses in this and all subsequent tables: the form of the anisotropic thermal ellipsoid is exp $-(B_{11}H^2 + B_{22}K^2 + B_{33}L^2 + 2B_{12}HK + 2B_{13}HL + 2B_{23}KL)$. The quantities given in the table are the thermal coefficients $\times 10^4$.

Table III. Positional and Thermal Parameters for the Atoms of $(Ir^{II}(H)(\mu\text{-Sr-Bu})(CO)(P(OCH_3)_3))_2$[a]

ATOM	X	Y	Z	B11 OR B(A²)	B22	B33	B12	B13	B23
IR	-0.21895(6)	0.17987(3)	0.22735(8)	4.77(6)	1.43(2)	8.72(9)	0.24(4)	0.74(5)	0.16(5)
S(1)	-0.4225(5)	1/4	0.2346(7)	5.0(6)	1.33(15)	11.2(10)	0	-0.7(6)	0
S(2)	-0.1860(6)	1/4	0.4906(7)	5.4(5)	2.61(20)	7.8(9)	0	0.2(6)	0
P	-0.2916(5)	0.07434(24)	0.3103(6)	8.0(5)	1.64(12)	20.5(11)	0.05(23)	1.6(6)	0.9(5)
O(1)	0.0628(12)	0.1310(8)	0.1414(16)	7.7(15)	5.0(6)	20.(3)	2.2(8)	4.5(17)	-1.0(11)
O(2)	-0.4500(12)	0.0679(7)	0.4139(17)	8.7(15)	3.3(5)	23.(3)	-1.4(7)	4.8(17)	2.1(10)
O(3)	-0.1754(14)	0.0365(8)	0.4341(21)	11.8(19)	3.4(6)	42.(5)	0.1(8)	-3.4(24)	7.3(14)
O(4)	-0.3397(16)	0.0172(7)	0.1730(16)	22.9(26)	2.3(5)	21.(3)	-2.8(9)	8.0(23)	-1.6(9)
C(1)	-0.0472(20)	0.1491(14)	0.1791(25)	9.9(25)	7.5(13)	12.(4)	2.0(14)	-3.4(24)	-8.8(16)
C(2)	-0.4438(24)	0.1102(12)	0.5638(20)	21.(4)	4.4(9)	15.(4)	-2.1(14)	12.(5)	-2.3(15)
C(3)	-0.2013(27)	-0.0314(14)	0.514(4)	21.(4)	4.7(11)	65.(11)	0.1(17)	-1.(5)	15.(5)
C(4)	-0.261(3)	0.0015(14)	0.027(4)	39.(7)	4.1(11)	37.(7)	-3.5(21)	24.(6)	-4.8(25)
C(5)	-0.5367(24)	1/4	0.037(3)	7.(3)	2.8(9)	15.(5)	0	-5.(5)	0
C(6)	-0.465(3)	1/4	-0.129(3)	12.(4)	6.6(17)	10.(5)	0	-3.(4)	0
C(7)	-0.6213(27)	0.3181(16)	0.048(3)	26.(5)	9.9(17)	33.(6)	12.3(24)	-19.(5)	-7.6(28)
C(8)	-0.0152(26)	1/4	0.614(3)	5.6(29)	6.2(15)	9.(5)	0	-0.5(29)	0
C(9)	0.1067(25)	1/4	0.498(4)	4.5(29)	6.6(15)	20.(6)	0	1.(5)	0
C(10)	-0.0134(22)	0.3167(16)	0.722(3)	10.8(28)	11.3(18)	27.(6)	0.1(19)	-4.(5)	-12.5(27)
H	-0.240	0.131	0.044	4.0					

[a] Estimated standard deviations in the least significant figure(s) are given in parentheses in this and all subsequent tables. The form of the anisotropic thermal ellipsoid is exp $-(B_{11}H^2 + B_{22}K^2 + B_{33}L^2 + 2B_{12}HK + 2B_{13}HL + 2B_{23}KL)$. The quantities given in the table are the thermal coefficients $\times 10^3$.

gives the corresponding dideuteride $[Ir(D)(\mu\text{-St-Bu})(CO)(PR_3)]_2$ which exhibits ν(IrD) in the 1520–1550-cm^{-1} region as expected.

The NMR data are consistent with all four complexes **2** (R = Me, Ph, NMe_2, and OMe) occurring in two isomeric forms, designated α and β (Table VII). The $^{31}P\{^1H\}$ NMR spectrum of **2** (R = Ph) at 36.4 MHz shows two singlets of unequal intensities at δ −12.71 (62%) and −11.76 ppm (38%) attributable, respectively, to the isomers β and α in which the phosphorus nuclei are equivalent.

The 90-MHz ^1H NMR spectra of **2** are temperature dependent, indicating a dynamic equilibrium between the two isomers. In the slow exchange region, they show two high-field triplets of unequal intensities attributable to isomers in which the hydrides are equivalent.

Let us consider, for example, the case **2** (R = OMe). In the slow exchange region (Figure 1) the spectrum exhibits one triplet for the phosphite protons (τ 6.35, $^3J_{PH}$ = 12.5 Hz), three singlets (checked also at 250 MHz) for the *tert*-butyl protons (τ 8.74, 8.67, 8.62), and two triplets of unequal intensities in the high-field region for the hydride proton (τ 25.45, $^2J_{PH}$ = 22.1 Hz; τ 24.60, $^2J_{PH}$ = 20.6 Hz). Integration of these three types of proton signals gives total areas in the expected ratios 18:18:2. The well-defined 1:2:1 "deceptively simple" triplet resonance due to the phosphite protons at τ 6.35 indicates a strong coupling between equivalent ^{31}P nuclei whereas this coupling appears to be very small in the starting compound **1** (R = OMe), from the shape of the ^1H spectrum (Figure 2). We thus expect the resonance signals of the equivalent hydrides of each isomer to appear as the X part of a second-order XAA′X′ spin system and this hypothesis is clearly verified by the nature of virtual 1:2:1 triplets of the hydride signals. The magnitudes of $^2J_{PH}$ indicate mutually cis hydride and phosphite ligands. On raising the temperature, the three *tert*-butyl singlets broaden and coalesce into one singlet whereas the two high-field virtual triplets broaden and coalesce into one triplet (τ 25.26, $^2J_{PH}$ = 20.6 Hz); the coalescence temperature, ca. 40 °C (90 MHz), was obtained from the hydride signal. The ratio α/β of the concentrations of the two isomers α and β, obtained below the coalescence temperature by integration of the hydride signals of each isomer, and above coalescence from the chemical shift of the time-averaged hy-

Table VI. Infrared Spectra for Complexes $(Ir(\mu\text{-St-Bu})(CO)(PR_3))_2$ (**1**), $(Ir(X)(\mu\text{-St-Bu})(CO)(PR_3))_2$ (**2**), and $\{Ir(X)(\mu\text{-St-Bu})(CO)(PR_3)_2(H)\}^+ClO_4^-$ (**3**)

compd	R	X	$\nu(CO)$,[a] cm^{-1}	$\nu(IrH)$,[a] cm^{-1}	$\nu(IrD)$,[b] cm^{-1}
1	Me		1955 (vs), 1941 (vs)		
	Ph		1965 (vs), 1951 (vs), 1935 (s)		
	NMe_2		1959 (vs), 1943 (vs)		
	OMe		1985 (vs), 1975 (vs), 1964 (vs)		
2	Me	H	1985 (vs), 1968 (sh), 1961 (vs)	2115	
	Ph	H	1989 (vs), 1972 (w), 1965 (w)	2132	
		D	1989 (vs), 1972 (w), 1965 (w)		1535
	NMe_2	H	2003 (w), 1987 (w), 1970 (vs)	2140	
	OMe	H	2007 (vs), 1992 (w), 1983 (m)	2128	
		D	2007 (vs), 1992 (w), 1983 (m)		1522
3	Me	H	2047 (vs),[c] 2030 (s)	2140[c]	
	Ph	H	2064 (vs),[c] 2051 (s)	2177[c]	
	OMe	H	2069 (vs),[c] 2057 (s)	2142[c]	
		D	2069 (vs),[c] 2057 (s)		1535

[a] Hexadecane solution. [b] Recorded as CsBr pellets. [c] Dichloromethane solution.

Table VII. ^1H (90 MHz) NMR Data[a] for Complexes $(Ir(\mu\text{-St-Bu})(CO)(PR_3))_2$ (**1**), $(Ir(X)(\mu\text{-St-Bu})(CO)(PR_3))_2$ (**2**) and $\{(Ir(X)(\mu\text{-St-Bu})(CO)(PR_3))_2(H)\}^+ClO_4^-$ (**3**)

				PR_3		t-Bu		H				
								terminal			bridging	
compd	R	X	solvent	τ	J_{PH}	τ	temp, °C	τ	$^2J_{PH}$	temp, °C	τ	$^2J_{PH}$
1	Me		C_7D_8	8.62 (d)	10.0	8.17						
						8.47						
2	Me	H	C_7D_8	8.44 (t)	9.0	8.6[b]	−20	α 27.25 (t)	16.2	−20		
								β 28.60 (t)	16.9			
								28.2[c]		+80		
2	Me	H	CH_2Cl_2[d]	8.24 (t)	9.0	α 8.73	−70	not measured				
						β {8.75, 8.78}						
						8.73	+38					
3	Me	H	$CDCl_3$	7.77 (t)	11.0	α 8.60		α 23.79 (t)	15.4		α 25.18 (t)	56.6
						β {8.56, 8.63}		β 24.11 (t)	17.6		β 25.09 (t)	55.2
1	Ph		CD_2Cl_2	2.9[c]		8.05						
						8.98						
2	Ph	H	CD_2Cl_2	2.55[c]		α 9.45	0	α 24.14 (t)	13.2	0		
						β {9.51, 9.54}		β 24.99 (t)	14.3			
3	Ph	H	$CDCl_3$	3.0[c]		α 9.33		α 23.21 (t)	15.4		α 25.04 (t)	55.1
						β {9.16, 9.39}		β 23.25 (t)	12.2		β 25.02 (t)	54.8
1	NMe_2		CD_2Cl_2	7.19 (d)	10.0	8.33						
						8.49						
2	NMe_2	H	$CDCl_2$	7.34 (t)	10.0	8.8[b]	0	α 26.87 (t)	20.9	0		
								β 27.39 (t)	26.6			
1	OMe		CD_2Cl_2	6.30 (d)	12.5	8.33						
						8.55						
2	OMe	H	$CDCl_3$	6.35 (t)	12.5	α 8.62	−40	α 24.60 (t)	20.6	−40		
						β {8.67, 8.74}		β 25.45 (t)	22.1			
						8.67	+55	25.26 (t)	20.6	+55		
2	OMe	H	C_7D_8	6.54 (t)	12.5	α 8.50	−30	α 24.23 (t)	19.1	−30		
						β {8.56, 8.67}		β 25.24 (t)	22.1			
						8.57	+60	24.97 (t)	20.6	+60		
3	OMe	H	$CDCl_3$	6.07 (t)	12.5	α 8.67		α 23.48 (t)	22.8		α 26.16 (t)	95.6
						β {8.60, 8.74}		β 23.60 (t)	22.8		β 26.12 (t)	93.4
3	OMe	D	$CDCl_3$	6.07 (t)	12.5	α 8.67					α 26.16 (t)	95.6
						β {8.60, 8.74}					β 26.12 (t)	93.4

[a] τ values ± 0.02, J values ± 0.2 Hz; α and β refer to the two isomeric forms discussed in the text. [b] Three badly resolved singlets. [c] Broad signal. [d] Recorded at 60 MHz on a Varian A-60 spectrometer.

dride signal, remains constant, ca. 5.7, between −40 and +80 °C.

A similar phenomenon was observed for compounds **2** (R = Me, Ph, and NMe_2).

All these results together with elemental analyses and molecular weights are clearly consistent with two isomeric configurations of the thiolato-bridged dihydridodiiridium complexes **2** in which one phosphine, one hydride, and one carbonyl

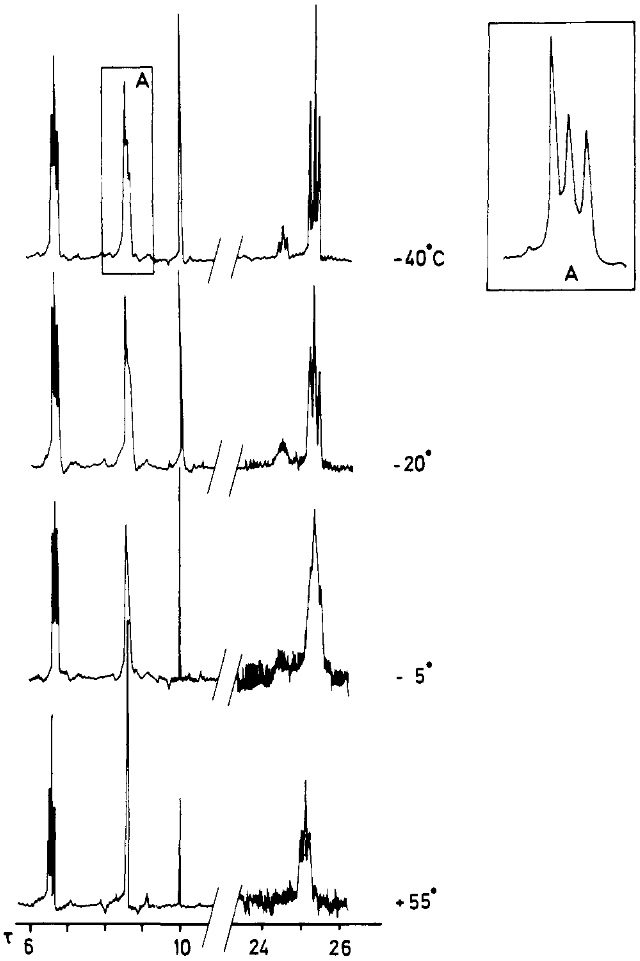

Figure 1. Temperature dependence of 90-MHz ^{1}H NMR spectrum of the complex **2** (R = OMe) in $CDCl_3$.

Figure 2. Comparison of the shapes of the OMe proton signals for the complexes **1** and **2** (R = OMe).

are bound to each iridium atom. The interaction between molecular hydrogen and complexes **1** may be formally interpreted as a one-electron oxidative addition to each metal atom. An electron pair coupling interaction between the two d^7 Ir^{II} atoms is then necessary in order for each iridium to attain a

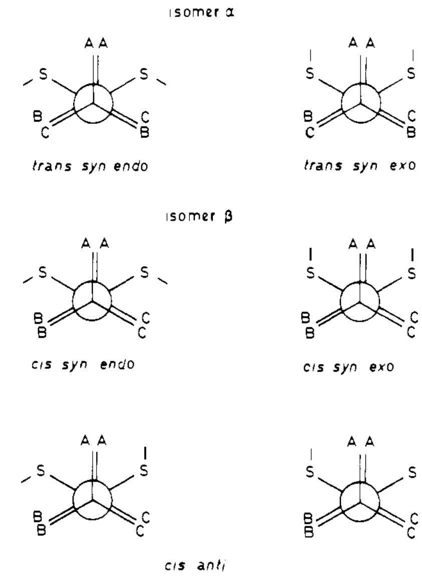

Figure 3. Possible configurations for the isomers α and β of **2**. These configurations take into account all the permutations of the ligands H, CO, and PR_3 at the sites A, B, and C.

closed-shell configuration, in accord with the diamagnetic character of these compounds **2**.

More information about the configurations of complexes **2** in solution can be deduced from vibrational spectra analysis of the dihydride and the dideuteride compounds. Since these two compounds exhibit identical CO stretching frequencies, the resonance interaction between ν(IrH) and ν(CO) modes is very weak. In contrast, important resonance interactions are observed for CO trans to H^{II} in Vaska-type complexes,[12] and our observations suggest a mutually cis disposition of the carbonyl and the hydride on each iridium atom.

Further structural information can be obtained from ^{1}H NMR spectra in the *tert*-butyl region. In the slow exchange region, three singlets very close together appear. The intensity ratios were obtained at 250 MHz. The isomer α must then be in one of the six possible configurations of the trans-syn type (Figure 3) in which each member of the pairs of ligands hydride, *tert*-butylthiolato, and phosphine are in equivalent positions. The other isomer, β, must be one of the 12 possible configurations of the cis-syn and cis-anti types in which the hydride protons and the phosphorus pairs are equivalent whereas *tert*-butyls are not.

Electronic Spectra. The UV-visible spectra of complexes **1** exhibit four well-defined absorption bands quite similar to those of mononuclear square-planar iridium(I) complexes containing π-acceptor ligands.[13] For example, the absorption spectrum of **1** (R = OMe) exhibits four bands at 445 nm (ε 4190 L mol^{-1} cm^{-1}), 385 (4410), 360 (4010), and 312 (4700). On addition of 1 mol of H_2 to 1 mol of **1** to give **2**, these four absorption bands progressively disappear and are replaced by a strong absorption, e.g., 322 nm (ε 10 070 L mol^{-1} cm^{-1}) for **2** (R = OMe) (Figure 4). For mononuclear planar iridium(I) complexes, the addition of H_2 to form six-coordinate complexes of iridium(III) leads to the quasi-complete disappearance of the absorption bands.[13a,c] A quite different result was obtained by Tolman et al.[14] in the case of $[Rh(\mu\text{-}Cl)(P(p\text{-}tolyl)_3)_2]_2$ for which the addition of 1 mol of H_2 at only one metal center to give $[Rh(\mu\text{-}Cl)(P(p\text{-}tolyl)_3)_2]_2(H)_2$ reduced the absorbance of the starting complex to about half its original value.

The intense bands in the 320–340-nm region may be correlated with the existence of metal-metal bonds in complexes **2**. Similar intense bands in this region have been observed for numerous d^7–d^7 metal-metal bonded complexes and are identified as dσ–dσ* transitions.[13c,15]

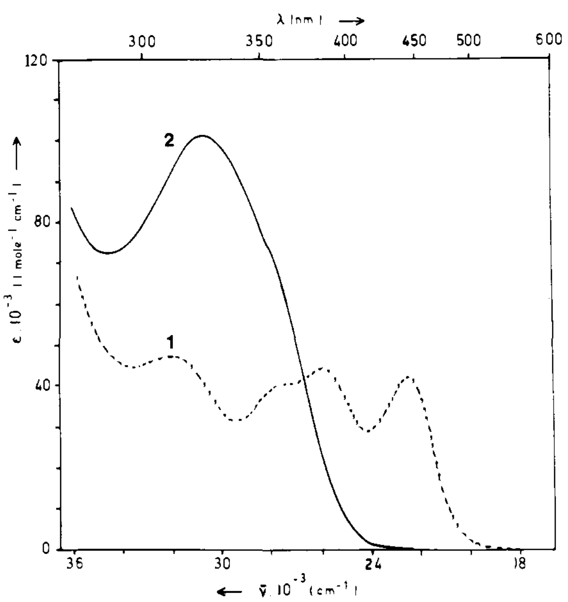

Figure 4. UV-visible absorption spectra of complexes **1** and **2** (R = OMe), in CH_2Cl_2, at 298 K.

Table VIII. Selected Bond Distances (Å) for **1** (R = OMe)

Ir(1)-Ir(2)	3.216 (2)	C(3)-C(6)	1.58 (4)
Ir(1)-S(1)	2.393 (9)	C(7)-C(8)	1.54 (4)
Ir(1)-S(2)	2.386 (9)	C(7)-C(9)	1.47 (5)
Ir(1)-P(1)	2.211 (9)	C(7)-C(10)	1.55 (5)
Ir(1)-C(1)	1.63 (4)	P(1)-O(3)	1.560 (19)
Ir(2)-S(1)	2.378 (9)	P(1)-O(4)	1.589 (27)
Ir(2)-S(2)	2.413 (9)	P(1)-O(5)	1.615 (20)
Ir(2)-P(2)	2.205 (12)	P(2)-O(6)	1.546 (27)
Ir(2)-C(2)	1.68 (5)	P(2)-O(7)	1.588 (27)
S(1)-C(3)	1.89 (3)	P(2)-O(8)	1.62 (3)
S(2)-C(7)	1.88 (3)	O(3)-C(11)	1.506 (37)
C(1)-O(1)	1.27 (4)	O(4)-C(12)	1.50 (4)
C(2)-O(2)	1.28 (5)	O(5)-C(13)	1.41 (3)
C(3)-C(4)	1.51 (4)	O(6)-C(16)	1.53 (4)
C(3)-C(5)	1.58 (4)	O(7)-C(15)	1.51 (5)
		O(8)-C(14)	1.33 (5)

Table IX. Selected Bond Angles (deg) for **1** (R = OMe)

S(1)-Ir(1)-S(2)	80.5 (3)	S(1)-Ir(2)-S(2)	80.2 (3)
S(1)-Ir(1)-P(1)	169.3 (3)	S(1)-Ir(2)-P(2)	170.6 (3)
S(1)-Ir(1)-C(1)	102 (1)	S(1)-Ir(2)-C(2)	101 (2)
S(2)-Ir(1)-P(1)	88.9 (3)	S(2)-Ir(2)-P(2)	90.4 (4)
S(2)-Ir(1)-C(1)	175 (1)	S(2)-Ir(2)-C(2)	176 (2)
P(1)-Ir(1)-C(1)	88 (1)	P(2)-Ir(2)-C(2)	88 (2)
Ir(1)-S(1)-Ir(2)	84.8 (2)	Ir(1)-S(2)-Ir(2)	84.2 (3)
Ir(1)-S(1)-C(3)	114 (1)	Ir(1)-S(2)-C(7)	118 (1)
Ir(2)-S(1)-C(3)	119 (1)	Ir(2)-S(2)-C(7)	112 (1)
Ir(1)-C(1)-O(1)	180 (3)		
Ir(2)-C(2)-O(2)	173 (4)		

Description of the Crystal and Molecular Structure of 1 (R = OMe). The crystal structure of **1** (R = OMe) consists of the packing of four dinuclear molecules. Bond distances are given in Table VIII and bond angles in Table IX. There is no close contact (< 3 Å) between dinuclear molecules. A perspective view of the molecule of **1** (R = OMe) including the labeling scheme is shown in Figure 5. The dinuclear molecule has roughly a mirror plane perpendicular to the Ir(1)-Ir(2) direction and containing the two sulfur bridging atoms. The geometry around each iridium atom is typical square planar for such dinuclear bridged d^8 metal complexes.[16] Each iridium is bonded to two sulfur atoms of *tert*-butylthiolato groups, one phosphorus atom of a trimethyl phosphite ligand, and one carbon atom of a carbonyl group. The phosphite and carbonyl ligands are in a cis arrangement. The dihedral angle between the two square planes is 123.2° and the Ir-Ir distance is 3.216 (2) Å. These values, expected from dinuclear d^8 complexes, have been extensively discussed in previous papers.[4,16] The angle between the two CO vectors is 83 (2)°.

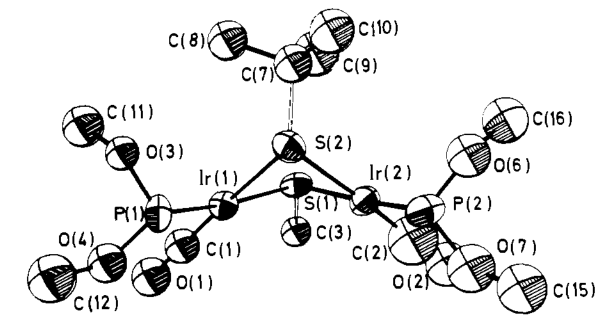

Figure 5. Perspective view of complex **1** (R = OMe). The methyls of one of the *t*-Bu groups, together with one OCH_3 group of each phosphite, have been omitted for clarity.

Table X. Selected Bond Distances (Å) for **2** (R = OMe)

Ir-Ir′	2.673 (1)	C(5)-C(7)	1.540 (25)
Ir-S(1)	2.368 (4)	C(8)-C(9)	1.539 (33)
Ir-S(2)	2.445 (5)	C(8)-C(10)	1.521 (25)
Ir-P	2.241 (4)	P-O(2)	1.619 (12)
Ir-C(1)	1.828 (19)	P-O(3)	1.596 (13)
		P-O(4)	1.570 (13)
S(1)-C(5)	1.837 (23)	O(2)-C(2)	1.431 (21)
S(2)-C(8)	1.865 (24)	O(3)-C(3)	1.467 (23)
C(1)-O(1)	1.176 (20)	O(4)-C(4)	1.444 (25)
C(5)-C(6)	1.508 (35)		

Table XI. Selected Bond Angles (deg) of **2** (R = OMe)

S(1)-Ir-S(2)	73.8 (2)
S(1)-Ir-P	102.9 (2)
S(1)-Ir-C(1)	161.6 (9)
S(2)-Ir-P	105.7 (2)
S(2)-Ir-C(1)	106.9 (5)
P-Ir-C(1)	94.6 (9)
Ir-S(1)-Ir′	68.7 (1)
Ir-S(2)-Ir′	66.3 (1)
Ir-S(1)-C(5)	115.7 (7)
Ir-S(2)-C(8)	118.8 (6)
Ir-C(1)-O(1)	177 (2)

Description of the Crystal and Molecular Structure of 2 (R = OMe). Isomerization of 2 in Solution. The crystal structure of **2** (R = OMe) consists of the packing of two dinuclear molecules. Bond distances are given in Table X and bond angles in Table XI. A perspective view of the molecule **2** (R = OMe), including the labeling scheme, is shown in Figure 6. The dinuclear molecule has a perfect mirror plane imposed by the $P2_1/m$ space group. This plane is perpendicular to the Ir-Ir′ direction and contains both sulfur bridging atoms, the tertiary carbons, i.e., C(5) and C(8), and one carbon of each *tert*-butyl group (i.e., C(6) and C(9)). The geometry around each iridium atom is of the rectangular pyramidal type if one considers the five nearest atoms around each iridium, i.e., two sulfur atoms of the *tert*-butylthiolato group, one phosphorus atom of a trimethyl phosphite, one carbon of a carbonyl group, and a hydrogen atom. The distances of the Ir atoms to the plane containing the two sulfur and the carbon C(1) atoms is 0.3 Å. The dinuclear molecule is achieved by the two sulfur atoms of the S *t*-Bu groups bridging the two iridium atoms. The phosphite ligand occupies the axial position and the Ir-P distance is 2.241 (4) Å. No very useful comparison for this bond distance can be made, since no Ir^{II}-P distance is available in the literature.

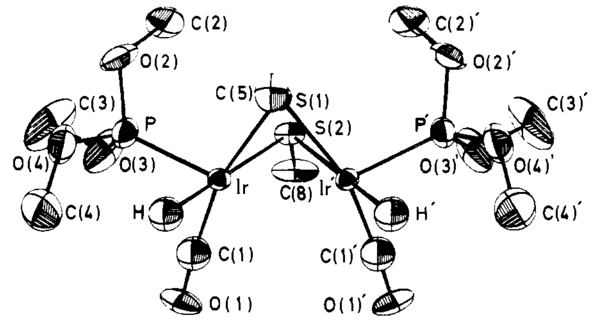

Figure 6. Perspective view of complex **2** (R = OMe). The methyls of the *t*-Bu groups have been omitted for clarity. Ellipsoids are drawn at a 50% level of probability. Primes denote atoms related to those in the asymmetric unit by the mirror plane perpendicular to the Ir–Ir′ axis and containing the two sulfur bridging atoms.

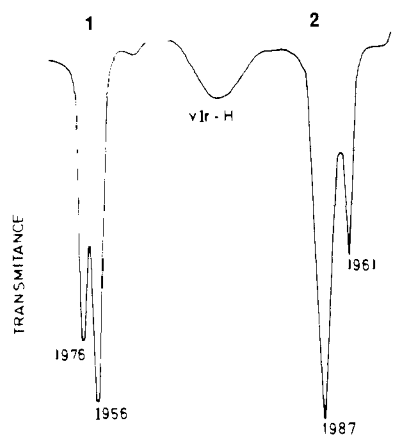

Figure 7. Infrared spectra in the 2200–1950-cm^{-1} region of **1** and **2** (R = OMe), in the solid state.

However, our observed distance is significantly shorter than the 2.309 Å found for $[IrH(\mu\text{-}SO_2)(CO)_2(PPh_3)]_2$[17] and the 2.279 (2) Å in $[Ir(\mu\text{-}PPh_2)(CO)(PPh_3)]_2$.[18] The Ir–S(2) bond distance of 2.445 (5) Å trans to the hydrido ligand is significantly longer than the Ir–S(1) of 2.368 (4) Å trans to the carbonyl group. This lengthening is the normal and well-known trans influence of the hydrido ligand.[19] The *t*-Bu groups are in this complex **2** (R = OMe) in a syn-endo configuration instead of the anti configuration in **1** (R = OMe). The dihedral angle between the two planes containing [Ir–S(1)–S(2)] and [Ir′–S(1)–S(2)] is 88.1° instead of 123.2° in complex **1** (R = OMe). The distance between the two iridium atoms, 2.673 (1) Å, indicates a normal two-electron Ir–Ir single bond as in bis(η^5-cyclopentadienyl)bis(carbonyl)-μ(*o*-phenylene)-diiridium(*Ir–Ir*)[20] in which the Ir··Ir distance is equal to 2.717 (1) Å. Moreover, other features in the present structure strongly indicate that a metal–metal bond is present: the acute angles at the S atoms, Ir–S(1)–Ir′ and Ir–S(2)–Ir′, of 68.7 (1) and 66.3 (2)°, respectively, are considerably smaller than the corresponding angles in compound **1** (R = OMe), i.e., 84.7 (3) and 84.1 (3)°, which does not exhibit a normal Ir–Ir bond. The acute dihedral angle between the [Ir–S(1)–S(2)] and [Ir′–S(1)–S(2)] planes of 88.1° (compared to 123.2° in **1** (R = OMe)) is indicative of considerable compression of the four-membered Ir_2S_2 ring along the Ir–Ir axis.

The angle between the two CO vectors is equal to 31 (3)° instead of 83 (2)° in **1** (R = OMe). The infrared spectra of crystalline compounds **1** and **2** (R = OMe) in which the structures have been described exhibit CO stretching bands (in cesium bromide pellets) at 1976 (I_{sym} = 48%) and 1956 (I_{asym} = 52%) cm^{-1} for the compound **1** (R = OMe) and 1987 (92%) and 1961 (8%) cm^{-1} for the compound **2** (R = OMe)

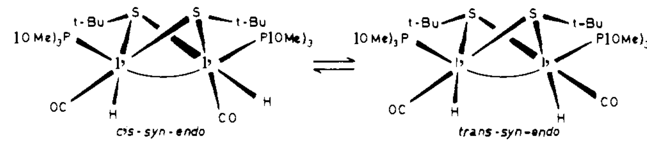

Figure 8. Stereochemistry of the isomers α and β of **2** (R = OMe).

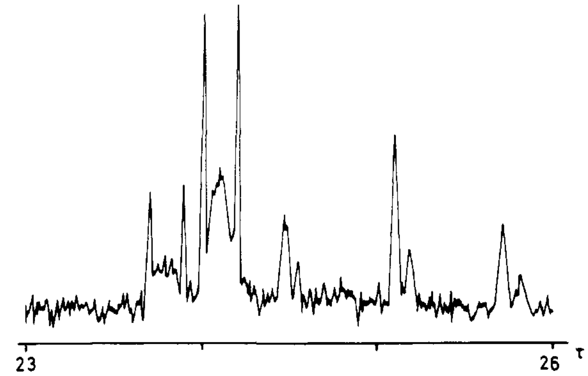

Figure 9. High-field ^1H (90 MHz) NMR spectrum of **3** (R = Me) in $CDCl_3$.

(Figure 7). According to the usual approximation in which each CO oscillator is treated as a dipole vector,[21] the calculated values for the angle between CO vectors in the compounds **1** and **2** (R = OMe), i.e., 92 and 33°, respectively, are consistent with the measured values, i.e., 83 (2) and 31 (8)°, and the ratio I_{sym}/I_{asym} is expected to give a very simple rough measurement of the compression of the four-membered Ir_2S_2 ring along the Ir–Ir axis when going from **1** to **2**.

The above X-ray structure determination identifies one of the isomers expected from NMR data (i.e., the cis-syn-endo (isomer β), τ_{OMe} 6.35 (t), $^3J_{PH}$ = 12.5 Hz; $\tau_{t\text{-Bu}}$ 8.67 (s) and 8.74 (s); τ_H 25.45 (t), $^2J_{PH}$ = 22.1 Hz). The other isomer (isomer α) is then necessarily the trans-syn (τ_{OMe} 6.35 (t), $^3J_{PH}$ = 12.5 Hz; $\tau_{t\text{-Bu}}$ 8.62 (s); τ_H 24.60 (t), $^2J_{PH}$ = 20.1 Hz). The shape of the central peaks of the high-field ^1H NMR signals reveals long-range J_{PP} couplings of the same magnitude for each isomer and is consistent with an apical position of the phosphite ligand in the case of the isomer α as in the case of the isomer β. An endo disposition of the *t*-Bu groups is also required by steric hindrance. The temperature dependence of the ^1H NMR signals indicates a dynamic equilibrium between these trans-syn-endo (α) and cis-syn-endo (β) isomers (Figure 8).

Protonation of the Iridium–Iridium Bonds in 2. The Ir–Ir bonds of **2** are open to attack by electrophilic reagents and we find[22] that the treatment of these complexes **2** by perchloric acid gives crystalline products of dimeric monocationic species $\{[Ir(H)(\mu\text{-St-Bu})(CO)(PR_3)]_2(H)\}^+ClO_4^-$, **3** (R = Me, Ph, OMe). A bridging position for the added proton is supported by the infrared spectra. The Ir–H vibration in the terminal region, which appears at 2142 cm^{-1} for **3** (R = OMe) (Table VI), is absent for the deuterium analogue $\{[Ir(D)(\mu\text{-St-Bu})(CO)(P(OMe)_3)]_2(H)\}^+ClO_4^-$ (obtained by protonation of the deuterated complex $[Ir(D)(\mu\text{-St-Bu})(CO)(P(OMe)_3]_2)$.

The ^1H NMR spectra of these compounds are invariant with temperature in the range −40 to +80 °C. The terminal hydride signals appear as two virtual triplets of unequal intensities (Figure 9). The coupling constants $^2J_{PH}$, in the range 12–23 Hz (Table VII), indicate that a terminal hydride ligand is cis to each phosphorus nucleus. The bridging hydride signals appear as a widely separated 1:2:1 triplet because each hydride is coupled equally to two equivalent phosphorus nuclei. The terminal virtual triplets are absent in the spectrum of the

Scheme I

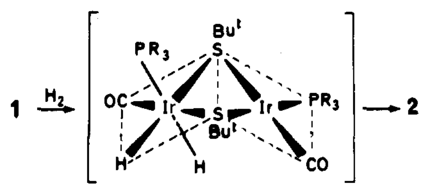

deuterated compound $\{[Ir(D)(\mu\text{-St-Bu})((CO)(P(OMe)_3)]_2(H)\}^+ ClO_4^-$. The coupling constant J_{PH}, in the range 55–95 Hz, rather suggests a trans disposition between the added proton and the phosphorus nuclei[23] and is quite consistent with a structure in which the phosphine ligands remain in an apical position as in the starting compounds. As expected, the proton resonance of methyl groups of the phosphine ligands is shifted to lower field with respect to the starting dihydride compounds. This signal appears as a virtual triplet and the shape of the central peak indicates a significant decrease of the ^{31}P–^{31}P coupling upon protonation. Such a decrease of the P–P coupling from **2** to **3** is also observed in the pattern of the terminal hydride signals.

The three singlets observed in the *t*-Bu region of the ^1H NMR spectra suggest the same two isomers as in the starting compounds **2** (i.e., one, cis-syn-endo, and the other, trans-syn-endo). There is no dynamic equilibrum, on the NMR time scale, between them, as judged by the invariance with temperature. Figure 10 depicts the stereochemistry of the protonation of the isomers α and β of complexes **2.**

The protonation reaction emphasizes the similarity of behaviors of compounds **2** and other dinuclear d^7–d^7 complexes[24] and is in perfect agreement with the previous structural descriptions. Moreover, from protonation of Fe^I complexes $[Fe(\mu\text{-SMe})(CO)_2(PMe_3)]_2$[25] giving $\{[Fe(\mu\text{-SMe})(CO)_2(PMe_3)]_2(\mu\text{-H})\}^+$, it has been shown that the protonation does not affect significantly the geometry of the dinuclear unit.[26]

Discussion

Pathway for the Formation and Isomerization of the Dihydridodiiridium Complexes 2. The formation of the dihydridodiiridium species **2** by a route in which each hydrogen atom of H_2 interacts with a different metal atom of **1** is evidently highly improbable. We suggest that the formation of **2** from **1** occurs by an intermediate Ir^{III}–Ir^I compound (called i_1) in which the

Scheme II

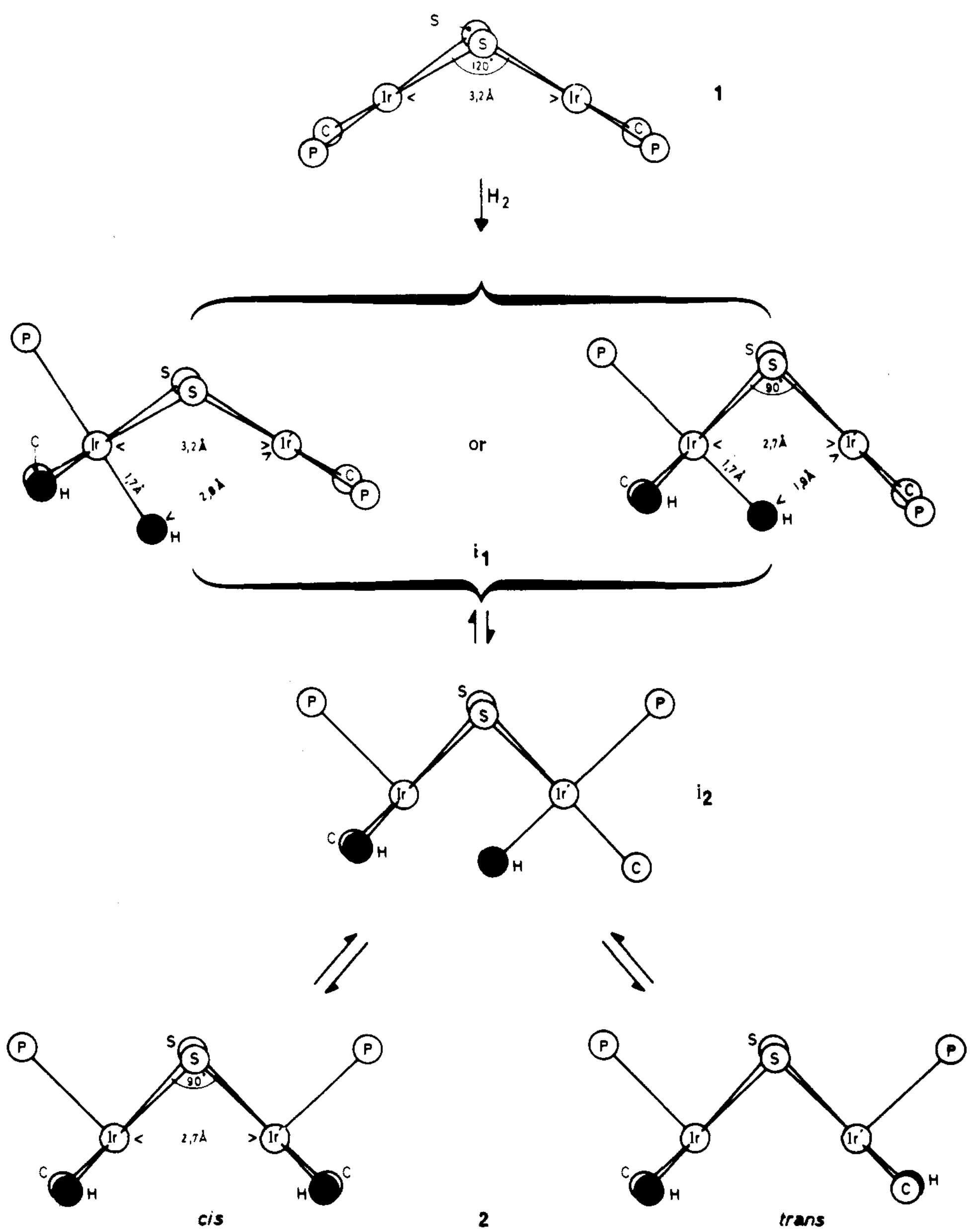

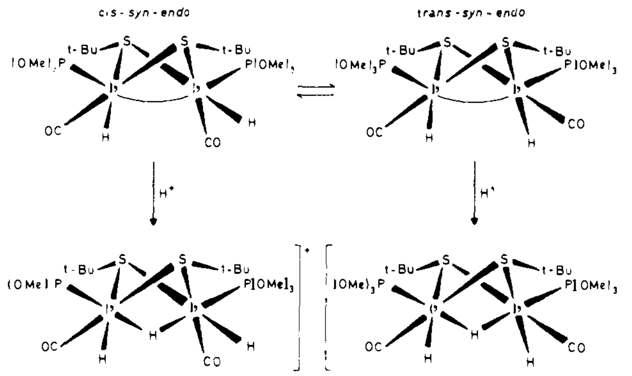

Figure 10. Stereochemistry of the protonation of the isomers α and β of complexes **2**.

two hydride ligands are bound to the same metal atom as in the case of the hydrogenated adduct of the complex $[RhCl(P(p\text{-tolyl})_3)_2]_2$.[14] The migration of one hydride from the Ir^{III} to the Ir^{I} center of i_1 may therefore be associated with the formation of the iridium-iridium bond (Scheme I).

Interconversion of cis and trans isomers can occur by bridge opening or by deformations of the geometry about metal atoms, the bridges remaining intact. Following several studies of isoelectronic $[(CO)_3Fe(\mu\text{-}PR_2)Fe(CO)_{3-n}L_n]$ complexes for which stereochemical nonrigidity was observed,[27] we tentatively propose a mechanism involving a formal Berry pseudorotation,[28] without bridge opening, as a route for inversion of molecules of **2** (if the geometry around each iridium is viewed as a square pyramid, ignoring the Ir-Ir bond).

It is of interest that one of the possible trigonal bipyramidal intermediates (called i_2) exhibits an axial hydride ligand very

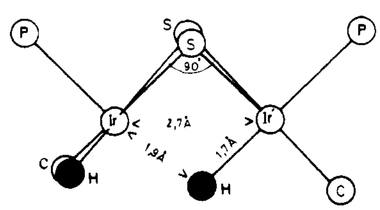

i_2

close to a bridging position between the Ir and Ir′ atoms, i.e., for Ir′-H = 1.7 Å, Ir-Ir′ = 2.7 Å, and a dihedral angle of the Ir-Ir′ axis $[IrS_2Ir'] = 90°$, the distance Ir-H in the complex i_2 is estimated to be 1.9 Å. This species i_2 would thus appear to approximate the species i_1 in which the two hydride ligands are bound to the same iridium atom. We think that it is attractive to consider i_1 and i_2 as two successive steps of the same elementary process which is common to the addition of H_2 to complexes **1** and to the cis-trans isomerization of complexes **2**. Scheme II illustrates the mechanism developed in the text. Two structures for the intermediate compound i_1 are proposed: they take into account the fact that i_1 may be closer than the starting material **1** or the dihydrido final compound **2**.

The assumption of such a mechanism is supported by the loss of fluxionality when a proton is added to the metal-metal bond. Moreover, the existence of an equilibrium between isomers α and β of **2** and the intermediate species i_1 is strongly suggested by the reactivity of **2** toward hexafluoro-2-butyne.[29] Indeed we have shown that the addition of C_4F_6 to solutions of complexes **2** (R = OMe, Me) gives quantitatively dissymmetric species $[(H)_2(PR_3)(CO)Ir(\mu\text{-St-Bu})_2Ir(CO)(PR_3)(C_4F_6)]$ in which the two hydride ligands are bound to one iridium atom and the alkyne is bound to the other.

We tentatively suggest that the migration of a hydride ligand from Ir^{III} to Ir^{I} is due to the existence of a coordinate covalent metal-metal bond in i_1, which brings the metallic centers closer together so that the apical hydride is near to a bridging position. Such metal-metal bonds have been proposed for the Ir^{I}-Ir^{III} interactions in $[(\eta\text{-}C_5Me_5)Ir_2(CO)_2(C_4F_6)_3H]$ (Ir-Ir = 2.737 (1) Å)[30] and $[(P(OMe)_3)_2(CO)Ir(\mu\text{-St-Bu})_2\text{-}Ir(CO)(TCNE)]$ (Ir-Ir = 2.679 (1) Å).[31]

Other evidence could be pointed out to support this hypothesis. The hydrogenation of $\{Rh(\mu\text{-}Cl)(P(p\text{-tolyl})_3)_2\}_2$ leads to a Rh^{I}-Rh^{III} species in which the two hydride ligands are coordinated to only one metallic center,[14] and the migration of the hydrogen atoms does not occur. However, the starting material does not have a bent geometry as found in our compounds **1** and its planar geometry[32] prevents the approach of the two metals and the formation of a compound analogous to **2**.

Acknowledgments. The authors would like to thank the CNRS, the D.G.R.S.T., and the D.E.S. for financial support.

Supplementary Material Available: Two listings of the observed and calculated structure factors amplitudes, Tables IV and V, of the root mean square amplitudes of vibration (12 pages). Ordering information is given on any current masthead page.

References and Notes

(1) Preliminary communication: Thorez, A.; Maisonnat, A.; Poilblanc, R. *J. Chem. Soc., Chem. Commun.* **1977**, 518–519.
(2) Muetterties, E. L. *Bull. Soc. Chim. Belg.* **1975**, *84*, 959–986. Ugo, R. *Catal. Rev.* **1975**, *11*, 225–297.
(3) Poilblanc, R. *J. Organomet. Chem.* **1975**, *94*, 241–250. *Nouveau J. Chim.* **1978**, *2*, 145–150.
(4) Bonnet, J. J.; Galy, J.; de Montauzon, D.; Poilblanc, R. *J. Chem. Soc., Chem. Commun.* 1977, 47–49.
(5) Mosset, A.; Bonnet, J. J.; Galy, J. *Acta Crystallogr., Sect. B* **1977**, *33*, 2639–2644.
(6) Cromer, D. T.; Waber, J. T. "International Tables for X-ray Crystallography", Vol. IV; Kynoch Press: Birmingham, England, 1974; Table 2.2.4. Cromer, D. T. *Ibid.*, Table 2.3.1.
(7) Cromer, D. T.; Ibers, J. A. In ref. 6.
(8) See paragraph at end of paper regarding supplementary material.
(9) The reductive elimination of H_2 does not take place by thermal activation under reduced pressure.
(10) In the case II (R = OMe), $\chi = -0.537 \times 10^{-3}$ cgs.
(11) Kaesz, H. D.; Saillant, R. B. *Chem. Rev.* **1972**, *72*, 231–281.
(12) Vaska, L.; Di Luzio, J. W. *J. Am. Chem. Soc.* **1962**, *84*, 679–680. Vaska, L. *Chem. Commun.* **1966**, 614–616. *J. Am. Chem. Soc.* **1966**, *88*, 4100–4101.
(13) (a) Strohmeier, W.; Muller, F. *Z. Naturforsch. B* **1969**, *24*, 770–772. (b) Geoffroy, G. L.; Wrighton, M. S.; Hammond, G. S.; Gray, H. B. *J. Am. Chem. Soc.* **1974**, *96*, 3105–3108. (c) Brady, R.; Flynn, B. R.; Geoffroy, G. L.; Gray, H. B., Peone, Jr., J.; Vaska, L. *Inorg. Chem.* **1976**, *15*, 1485–1488. (d) Geoffroy, G. L.; Isci, H.; Litrenti, J.; Mason, W. R. *Ibid.* **1977**, *16*, 1950–1955. (e) Levenson, R. A.; Gray, H. B.; Ceasar, G. P. *J. Am. Chem. Soc.* **1970**, *92*, 3653–3658.
(14) Tolman, C. A.; Meakin, P. Z.; Lindner, D. L.; Jesson, J. P. *J. Am. Chem. Soc.* **1974**, *96*, 2762–2774.
(15) Levenson, R. A.; Gray, H. B. *J. Am. Chem. Soc.* **1975**, *97*, 6042–6047. Lewis, N. S.; Mann, K. R.; Gordon II, J. G.; Gray, H. B. *Ibid.* **1976**, *98*, 7461–7463. Jackson, R. A.; Poe, A. *Inorg. Chem.* **1978**, *17*, 997–1003. Abrahamson, H. B.; Wrighton, M. S. *Ibid.* **1978**, *17*, 1003–1008.
(16) Bonnet, J. J.; Jeannin, Y.; Kalck, P.; Maisonnat, A.; Poilblanc, R. *Inorg. Chem.* **1975**, *14*, 743–747. Bonnet, J. J.; Kalck, P.; Poilblanc, R. *Ibid.* **1977**, *16*, 1514–1518. Bonnet, J. J.; de Montauzon, D.; Galy, J.; Poilblanc, R. *Acta Crystallogr.*, in press.
(17) Angoletta, M.; Bellon, P. L.; Manossero, M.; Sansoni, M. *J. Organomet. Chem.* **1974**, *81*, C40–C42.
(18) Mason, R.; Sotofte, I.; Robinson, S. D.; Uttley, M. F. *J. Organomet. Chem.* **1972**, *46*, C61–C62.
(19) Frenz, B. A.; Ibers, J. A. "Transition Metal Hydrides", Muetterties, E. L., Ed.; Marcel Dekker: New York, 1971; pp 41–44.
(20) Rausch, M. D.; Gastinger, R. G.; Gardner, S. A.; Brown, R. K.; Wood, J. S. *J. Am. Chem. Soc.* **1977**, *99*, 7870–7876.
(21) Cotton, F. A.; Wilkinson, G. "Advanced Inorganic Chemistry," 3rd ed.; Wiley-Interscience: New York, 1972; pp 693–701.
(22) Preliminary communication: Thorez, A.; Maisonnat, A.; Poilblanc, R. *Inorg. Chim. Acta* **1977**, *25*, L19–L20.
(23) Crabtree, R. H.; Felkin, H.; Morris, G. E. *J. Organomet. Chem.* **1977**, *141*, 205–215.
(24) Harris, D. C.; Gray, H. B. *Inorg. Chem.* **1975**, *14*, 1215–1217. Fauvel, K.; Mathieu, R.; Poilblanc, R. *Ibid.* **1976**, *15*, 976–978.
(25) Leborgne, G.; Grandjean, D.; Mathieu, R.; Poilblanc, R. *J. Organomet. Chem.* **1977**, *131*, 429–438.
(26) Savariault, J. M.; Bonnet, J. J.; Mathieu, R.; Galy, J. *C. R. Acad. Sci., Ser. C* **1977**, *284*, 663–665.
(27) Adams, R. D.; Cotton, F. A. *J. Am. Chem. Soc.* **1970**, *92*, 5003–5004.

Adams, R. D.; Cotton, F. A.; Cullen, W. R.; Hunter, D. L.; Mihichuk, L. *Inorg. Chem.* **1975**, *14*, 1395–1399. Flood, T. C.; Di Santi, F. J.; Campbell, K. D. *Ibid.* **1978**, *17*, 1643–1646.
(28) Berry, R. S. *J. Chem. Phys.* **1960**, *32*, 933–938.
(29) Maisonnat, A.; Poilblanc, R. *J. Organomet. Chem.* **1978**, *160*, 307–317.
(30) Corrigan, A.; Dickson, R. S.; Fallon, G. G.; Michel, K. J.; Mok, C. *Aust. J. Chem.* **1978**, *31*, 1937–1951.
(31) Bonnet, J. J.; Maisonnat, A.; Poilblanc, R., to be published.
(32) Curtis, M. D.; Butler, W. M.; Greene, J. *Inorg. Chem.* **1978**, *17*, 2928–2931.

A Comparative Study of the Reactions of *F*-(*tert*-Butyl) Hypochlorite and *F*-Methyl Hypochlorite with Simple Sulfur Compounds

Qui-Chee Mir, Kirk A. Laurence,[1] Robert W. Shreeve, Daniel P. Babb,[2] and Jean'ne M. Shreeve*

Contribution from the Department of Chemistry, University of Idaho, Moscow, Idaho 83843. *Received March 19, 1979*

Abstract: While CF_3SCF_3, $CF_3S(O)CF_3$, and SF_4 readily undergo oxidative addition with CF_3OCl to form $(CF_3)_2S(OCF_3)_2$, $(CF_3)_2S(O)(OCF_3)_2$, and $SF_4(OCF_3)_2$, no reaction is observed with $(CF_3)_3COCl$. On the other hand, CF_3SCl and SCF_2SCF_2 are reacted with $(CF_3)_3COCl$ to yield $CF_3S(OC(CF_3)_3)_2Cl$ (A) and $CF_2SCF_2S(OC(CF_3)_3)_2$ (E). *F*-Methyl hypochlorite adds two CF_3O groups to each sulfur in SCF_2SCF_2. With $CF_3S(O)Cl$, oxidative displacement of chlorine with $(CF_3)_3COCl$ forms $CF_3S(O)OC(CF_3)_3$ (B). In reaction with SCl_2 or CCl_3SCl, both oxidative displacement and oxidative addition occur with $(CF_3)_3COCl$ to give the tetrakis derivative, $S(OC(CF_3)_3)_4$ (D). Unsymmetric oxidative addition to a single sulfur in CF_3SSCF_3 occurs with $(CF_3)_3COCl$ to prepare $CF_3S(OC(CF_3)_3)_2SCF_3$ (C). With CF_3SCl, $CF_3S(O)Cl$, SCl_2, and CF_3SSCF_3, CF_3OCl assumes the role of fluorinating reagent. Neither hypochlorite was found to react with $(CF_3)_2SF_2$.

In recent papers, we have demonstrated that *F*-methyl hypochlorite is an excellent F-methoxylating reagent with acyclic and cyclic sulfur(II)- and -(IV)-containing compounds,[3,4] viz., eq 1 and 2. Earlier, others had studied the in-

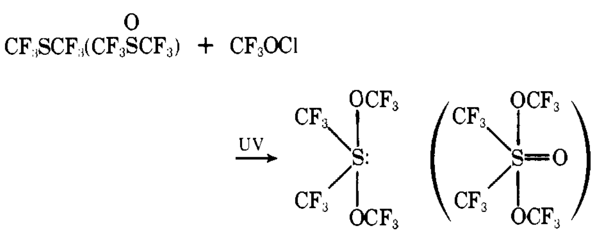
(1)

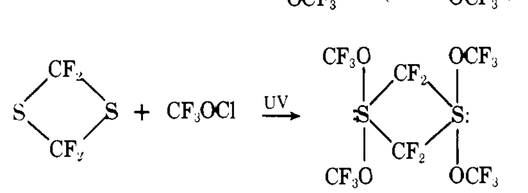
(2)

sertion of olefins[5–7] into the O–Cl bond of a variety of R_FOCl compounds (R_F = CF_3, $i\text{-}C_3F_7$, $(CF_3)_3C$–, SF_5–) to form fluorocarbon ethers with excellent thermal stability, especially in the case of perhalofluorinated materials. Small molecules or atoms, such as SO_2,[8,9] CO,[9] and Hg,[10] also insert into the O–Cl bond to form chlorosulfates, chloroformates, and a reactive mercurial. This type of insertion reaction is in contrast to the oxidative addition in reactions 1 and 2 where, if insertion does occur, a subsequent reaction must take place to replace the chlorine by a second *F*-methoxy group.

In another reaction mode, Fox and co-workers have shown that *F*-(*tert*-butoxy)phosphoranes and *F*-(*tert*-butoxy)boranes result from oxidative displacement of chlorine from $PClF_4$ and PCl_2F_3,[11] and from BCl_3[12] by $(CF_3)_3COCl$. While exploring the versatility of *F*-(*tert*-butyl) hypochlorite as a synthetic reagent, we were impressed by the marked difference in chemical behavior and concomitant products obtained when compared with our observations for *F*-methyl hypochlorite in analogous reactions.

Results and Discussion

In Table I are listed the reaction products obtained when CF_3OCl or $(CF_3)_3COCl$ is reacted with a variety of simple sulfur compounds and with mercury. Insertion of mercury into the OCl bond of $(CF_3)_3COCl$ and the concomitant formation of a stable mercurial[10] are in keeping with the behavior exhibited by other small molecules cited above. Also, the lability of the fluorine on the α carbon is a well-known phenomenon, and it is therefore not surprising that CF_3OCl undergoes slow decomposition in the presence of mercury to form COF_2 and HgClF.

However, it is surprising that, when $(CF_3)_3COCl$ is reacted with CF_3SCl, a new stable chloro-*F*-methylbis(*F*-butoxy)-sulfurane results, but with $CF_3S(O)Cl$ chlorine displacement occurs. The compounds CF_3SCl[13] and $CF_3S(O)Cl$[14a–d] undergo hundreds of reactions which support the polarity $CF_3S^{\delta+}Cl^{\delta-}$ and $CF_3S(O)^{\delta+}Cl^{\delta-}$ and which lead us to expect permanent loss of the sulfur-chlorine bond in each case. The new sulfurane is stable indefinitely at 0 °C and for limited periods at 25 °C. It is the first example of such an acyclic compound which is isolable at 25 °C. We had reported[15] earlier the chlorosulfurane and chlorosulfurane oxide, $CF_3S(NR_2)_2Cl$ and $CF_3S(O)(NR_2)_2Cl$, which are stable at 25 °C and above. The former was slowly hydrolyzed to $CF_3S(O)NR_2$, but $CF_3S(O)(NR_2)_2Cl$ was stable to hydrolysis in H_2O at 25 °C.

Chlorosulfuranes are in general much less stable than fluorosulfuranes. Several have been suggested as reaction intermediates without isolation,[16a–e] while those which have been isolated are unstable toward hydrolysis[17a–d] and thermolysis at 25 °C. By taking advantage of the enhanced stability of monocyclic and spirosulfuranes compared to acyclic sulfuranes, Martin and co-workers[17a,18] isolated a monocyclic

0002-7863/79/1501-5949$01.00/0